JOURNAL OF CHEMICAL INFORMATION AND MODELING

Article

pubs.acs.org/jcim

New Group IV Chemical Motifs for Improved Dielectric Permittivity of Polyethylene

G. Pilania,[†] C. C. Wang,[†] K. Wu,[§] N. Sukumar,[§,⊥] C. Breneman,[§] G. Sotzing,[‡] and R. Ramprasad*[,†]

[†]Chemical, Materials, and Biomolecular Engineering and [‡]Department of Chemistry and the Polymer Program, Institute of Materials Science, University of Connecticut, Storrs, Connecticut 06269, United States

[§]Rensselaer Exploratory Center for Cheminformatics Research and Department of Chemistry and Chemical Biology, Rensselaer Polytechnic Institute, Troy, New York 12180, United States

[⊥]Department of Chemistry and Center for Informatics, Shiv Nadar University, Dadri, India

Supporting Information

ABSTRACT: An enhanced dielectric permittivity of polyethylene and related polymers, while not overly sacrificing their excellent insulating properties, is highly desirable for various electrical energy storage applications. In this computational study, we use density functional theory (DFT) in combination with modified group additivity based high throughput techniques to identify promising chemical motifs that can increase the dielectric permittivity of polyethylene. We consider isolated polyethylene chains and allow the CH_2 units in the backbone to be replaced by a number of Group IV halides (viz., SiF_2, $SiCl_2$, GeF_2, $GeCl_2$, SnF_2, or $SnCl_2$ units) in a systematic, progressive, and exhaustive manner. The dielectric permittivity of the chemically modified polyethylene chains is determined by employing DFT computations in combination with the effective medium theory for a limited set of compositions and configurations. The underlying chemical trends in the DFT data are first rationalized in terms of various tabulated atomic properties of the constituent atoms. Next, by parametrizing a modified group contribution expansion using the DFT data set, we are able to predict the dielectric permittivity and bandgap of nearly 30 000 systems spanning a much larger part of the configurational and compositional space. Promising motifs which lead to simultaneously large dielectric constant and band gap in the modified polyethylene chains have been identified. Our theoretical work is expected to serve as a possible motivation for future experimental efforts.

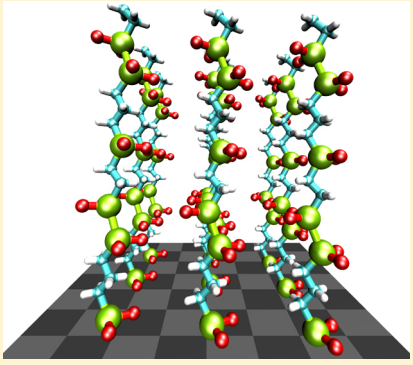

I. INTRODUCTION

The rational design of new materials with attractive properties hinges on our ability to intentionally modify the chemical structure of materials in ways that could directly impact their properties. While this discovery process has largely been guided by experimental efforts in the past, the in silico design of new materials using electronic-structure calculations is increasingly being seen as an attractive alternative option.[1−6] An important ingredient in most such successful in silico attempts is the careful extraction of chemical trends and insights from carefully planned large-scale high-throughput computations spanning a diverse range of chemical situations.[1−27]

In this article, we consider chemical modifications of polyethylene with an intent to enhance its dielectric properties without overly sacrificing its already remarkable insulating characteristics. Such an intentional modification may impact applications where insulators with high dielectric constant are required, such as in high energy density capacitors where polyethylene and polypropylene based systems (which have a low dielectric constant) are currently the standard materials,[28−35] as well as in electronic devices.[36−38]

Our in silico chemical modification of individual polyethylene chains involves the replacement of the CH_2 building units of polyethylene by the Group IV halides, including SiF_2, $SiCl_2$, GeF_2, $GeCl_2$, SnF_2, and $SnCl_2$, in a systematic, progressive, and exhaustive combinatorial manner, subjected to constraints imposed by the requirements of periodicity, system size, and stability. The motivation behind substituting C with the larger Group IV elements (i.e, Si, Ge, and Sn) in the polymer backbone is to ensure chemical compatibility by preserving the local chemical environment and bonding as well as to insert more polarizable units than C in the backbone that would result in an enhanced dielectric response.[39,40] Furthermore, constraining the side chain pendent groups to small atoms with high electronegativity such as F and Cl would provide large dipole moments that would not only contribute to the orientational part of the dielectric permittivity but are also expected to preserve the insulating behavior.

We are primarily interested in motifs that would provide a large dielectric constant in combination with a large bandgap (for ensuring good insulating properties) upon their incorporation in polyethylene. We further note that a larger bandgap generally correlates to a larger intrinsic breakdown field

Received: January 16, 2013
Published: March 22, 2013

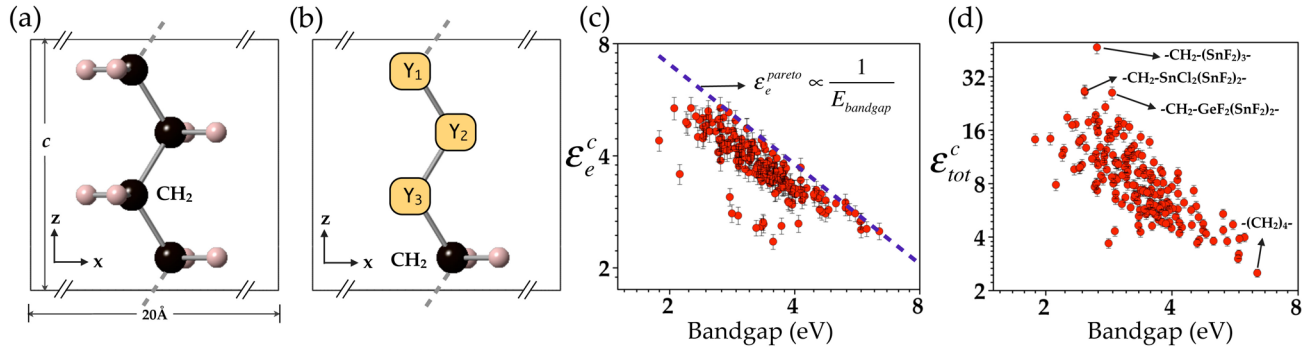

Figure 1. (a) Atomistic model of an all-trans single polyethylene chain containing four independent CH_2 units. (b) Schematic representation of the general model that was used to generate 175 systems for DFT computations by independently filling up the three places (i.e., Y_1, Y_2, Y_3) in the backbone with any of the seven CH_2, SiF_2, $SiCl_2$, GeF_2, $GeCl_2$, SnF_2, and $SnCl_2$ units. The DFT computed (c) electronic (ε_e^c) and (d) total (ε_{tot}^c) dielectric permittivities as a function of the computed DFT bandgap for the 175 systems.

strength, desirable for many dielectric and electrical applications. Therefore, our theoretical investigation starts with computations of the electronic structure and dielectric permittivities of a limited set of chemically modified and well-isolated polyethylenelike chains using first principles methods. To better understand the relative chemical trends in the DFT data, we search for possible correlations between the calculated properties and several atomic properties of the constituent atoms. Interestingly, the electronic and the total dielectric permittivities can be rationalized, respectively, in terms of the total atomic polarizability per unit volume and the magnitude of the local dipole moments that can be easily reoriented. Inspired by these trends, the DFT data was used to develop a parametrization based on additive group contributions[43] to explore a larger part of the compositional and configurational space spanning almost 30 000 systems. Interestingly, our analysis shows that the chemical space of the systems that provide simultaneously large bandgap and high dielectric permittivity is mainly composed of fluorides. Furthermore, we also find that the relative positions of various units (i.e., the chain configuration) has a significant effect on the properties. For instance, our results suggest that incorporation of motifs containing contiguous SnF_2 or GeF_2 units in polyethylene (with their number fraction in a suitable range) is expected to lead to superior dielectric permittivities.

We believe that the insights and knowledge drawn from our systematic theoretical exploration would serve as a possible motivation for synthesis efforts involving Group IV fluoride motifs in organic polymers, thereby adding to the already rich literature on organo-silicon, organo-germanium, and organo-tin based molecular chemistries.[44−47] Below we describe our theoretical analysis in greater detail.

II. MODEL AND METHODS

Our computations were performed within the DFT[48−50] framework using a generalized gradient approximation (GGA) functional parametrized by Perdew Burke and Ernzerhof (PBE).[51] The Vienna ab initio software package (VASP)[52] was used with the projector augmented wave (PAW) pseudopotentials,[53] and plane-wave basis functions up to a kinetic energy cutoff of 500 eV.

Infinitely long isolated all-trans polyethylene chains containing four independent CH_2 units (c.f. Figure 1a) in a supercell were simulated using periodic boundary conditions. While at least one CH_2 unit was always retained in the backbone to break the extent of σ-conjugation along the backbone (and to preserve some semblance of polyethylene), three places in the backbone schematically depicted as Y_1, Y_2, and Y_3 in Figure 1b, were filled by drawing from the following "pool" of seven possibilities: CH_2, SiF_2, $SiCl_2$, GeF_2, $GeCl_2$, SnF_2, and $SnCl_2$. This scheme resulted in 175 symmetry unique systems after accounting for translational periodicity. A vacuum of at least 20 Å normal to a polymer chain (i.e., along the x and y directions) was used to minimize spurious unphysical interactions between the periodic images. A Monkhorst−Pack k-point mesh of $1 \times 1 \times k$ (with $kc > 50$) produced converged results for a supercell of length c Å along the chain direction (i.e., the z direction). The supercells were relaxed using a conjugate gradient algorithm until the forces on all atoms were <0.02 eV/Å, and the stress component along the z direction was $<1.0 \times 10^{-2}$ GPa. Sufficiently large grids were used to avoid so-called "wrap-around" errors in fast Fourier transforms.

Although accurate dielectric properties of materials are readily accessible today through density functional perturbation theory (DFPT),[54,55] such a conventional approach requires a priori knowledge of the appropriate crystal structure for all material candidates to be investigated. If one is interested in a large part of the chemical space, determination of a global minimum on the potential energy surface for each of the new systems to be investigated may not be a practically feasible solution. Toward this end, here we use our newly developed method[40,56] to estimate the dielectric permittivity of pristine and chemically modified polyethylene. This approach requires only a knowledge of the individual chain structure, but not the manner in which the chains are packed together. The dielectric permittivity of an isolated polymer chain placed in a large supercell with a total volume V_{tot} is first computed using DFPT and includes contributions from the polymer as well as from the surrounding vacuum region of the supercell. Next, treating the supercell as a vacuum−polymer composite, effective medium theory[57] is used to estimate the dielectric constant of just the polymer.

According to the Maxwell−Garnett equation, the principal components of dielectric constant of a vacuum-filler composite (ε_{ii}) containing a volume fraction η_v of polarizable fillers (polymer chain in this case with dielectric constant, $\varepsilon_{ii}^{polymer}$) can be written as[57]

$$\frac{\varepsilon_{ii} - 1}{1 + (\varepsilon_{ii} - 1)P_i} = \eta_v \frac{\varepsilon_{ii}^{polymer} - 1}{1 + (\varepsilon_{ii}^{polymer} - 1)P_i} \quad (1)$$

dx.doi.org/10.1021/ci400033h | J. Chem. Inf. Model. 2013, 53, 879−886

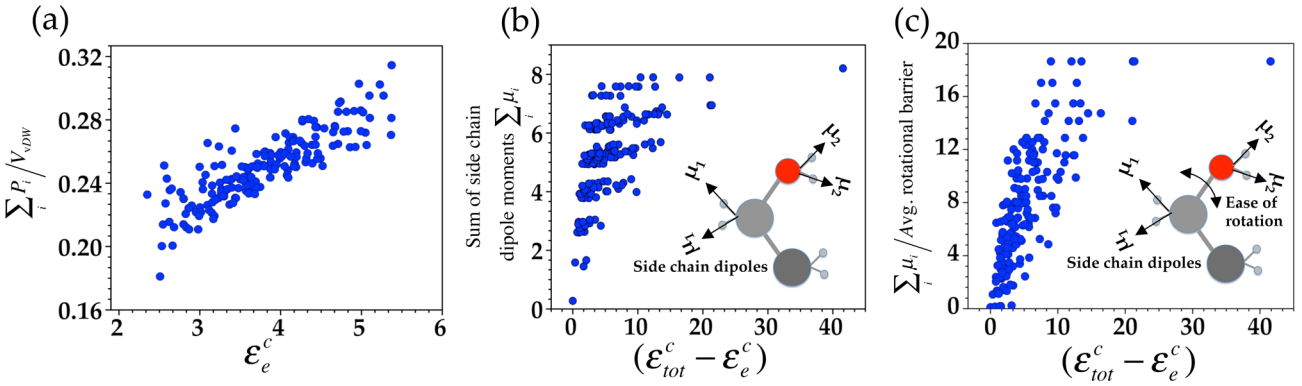

Figure 2. Correlations between the DFT computed data (abscissas) and various atomic properties of the constituent atoms (ordinates). (a) Correlation between the electronic part of the dielectric constant and the sum of the atomic polarizabilities of all the atoms ($\sum P_i$) in the system divided by the van der Waals volume (V_{vdW}) of the polymer chains. (b and c) Dependence of of the ionic part of the dielectric constant on the bond dipole moments of the side chain pendent groups ($\sum \mu$) and their relative ease of reorientation around the backbone. Please see text for details.

Here i represents the Cartesian axes x, y, or z, and P_i is a geometry-dependent depolarizing factor.[58−60] For the case at hand, since the polymer chains are oriented along the z direction, there are no depolarizing fields along the direction of periodicity; i.e., $P_z = 0$. This leads to the following formula for the axial component of the dielectric constant:[61,62]

$$\varepsilon_{zz} = \eta_v(\varepsilon_{zz}^{\text{polymer}} - 1) + 1 \quad (2)$$

In the above equations, η_v (= $V_{\text{polymer}}/V_{\text{tot}}$) is the volume fraction of the polymer in the supercell, which needs to be quantified to estimate the dielectric constant of just the polymer, i.e., $\varepsilon_{ii}^{\text{polymer}}$. Here, a procedure based on electronic charge density cutoffs is used to estimate the volume. While moving away from the polymer chain in the supercell, a region is deemed to be occupied by the polymer until the electronic charge density falls below a cutoff value. Our analysis based on a number of conventional polymers (for which reliable experimental densities are available, including polyethylene, polypropylene, polyacetylene, polythiophene, polypyrole, polydimethylsiloxane) showed that a charge density cutoff between the 3×10^{-3} and 7×10^{-3} e/Å^3 range is required to reproduce the experimental densities. We further note that this range of charge density cutoffs results in a range of volumes, V_{polymer}, which in turn translates to (rather small) error bars in the dielectric constants calculated using eq 2. We further note here that while the dielectric permittivity along the axial direction can be computed reliably using our single-chain method, the accuracy of the dielectric constant along the off-axis directions may be limited by the neglect of interchain interactions (although qualitative trends are still well-captured by this approach).[40] We thus focus mainly on the axial component of the dielectric constant in the present study.

As the insulating behavior of a dielectric correlates with the band gap (as does the intrinsic dielectric breakdown strength[41,42]), we also monitor the band gap of our polymeric chains as a function of chemical modifications. In the present work, we compute, and present, the band gap computed at the PBE level of theory. We further note that owing to the well-known tendency of semilocal DFT to underestimate the electronic bandgaps,[63] the bandgaps presented here are expected to provide a lower bound for the corresponding real bandgaps.

III. RESULTS AND DISCUSSION

A. Chemical Trends in the DFT Data. Table 1 of the Supporting Information contains the quantities determined using our DFT computations for all 175 systems, including the optimized c lattice parameters, the formation energies, the bandgap, and the dielectric constant values along the chain axis (electronic, ε_e^c, and total, ε_{tot}^c, contributions). All the 175 systems found to be thermodynamically stable against decomposition into the respective standard elemental states and represent a local minimum on the potential energy hypersurface as confirmed by normal-mode analysis. Figure 1c portrays the dependence of ε_e^c on the bandgap. While the pristine polyethylene chain has the highest calculated bandgap among all the systems explored, additions of the larger Group IV elements to the chain lead to a progressive decrease in the bandgap. A near-perfect inverse Pareto optimal front relationship (indicated as the dashed line) between the ε_e^c and the bandgap can be seen from Figure 1c. This inverse relationship[64] may be understood by realizing that the irreducible polarizability matrix of a system can be written as a sum over electronic transitions from the valence to conduction band manifolds with the corresponding transition energies appearing in the denominator.[65] It is thus evident that restrictions exist in the degree to which the electronic part of the dielectric constant can be enhanced.

Figure 1d shows the variation of the bandgap with the ε_{tot}^c. The ε_{tot}^c derives its contributions from the electronic polarization as well as the lattice mode vibrations and spans over a large range between 2.5 to 47, with the smallest and largest values corresponding to $-(CH_2)_4-$ and $-CH_2-(SnF_2)_3-$ motifs, respectively. In general, it is found that for a given composition and configuration, as the X in an XY_2 unit varies from C to Si to Ge to Sn (while all the other units in the chain are held fixed), both the ε_e^c and ε_{tot}^c increase and the bandgap decreases.

To better understand the DFT data, we attempt to correlate the observed chemical trends in the data to various tabulated *atomic* properties of the constituent units. The results of our analysis are collected in Figure 2. We find that the electronic part of the dielectric constant is strongly correlated with the sum of the polarizabilities of all the atoms in the system ($\sum P_i$) and is inversely proportional to van der Waals volume (V_{vdW}) of the polymer chains, as shown in Figure 2a. This knowledge leads us to a general conclusion that small (i.e., more compact)

dx.doi.org/10.1021/ci400033h | J. Chem. Inf. Model. 2013, 53, 879−886

constituent units with large atomic polarizability lead to a larger electronic part of the dielectric constant.

The ionic part of the dielectric permittivity is expected to depend on both the presence of structural units with large dipole moments and their ability to easily reorient themselves along the direction of the applied external field. In Figure 2b, we plot the total bond dipole moments ($\sum\mu_i$), contributed by the bonds between the backbone atoms and the side-chain atoms, versus the ionic part of the dielectric permittivity. The bond dipole moment of an X−Y bond is defined using Pauling's electronegativity (χ) as follows[66]

$$\mu = ed\left(1 - \exp\frac{-(\chi_X - \chi_Y)^2}{4}\right) \tag{3}$$

where e and d are electronic charge and the X−Y bond length, respectively. The bond length d was estimated by the sum of the covalent radii of atoms X and Y. Note that owing to the small electronegativity differences between the Group IV elements, the dipole moments arising due to the bonds along the backbone are expected to be quite small and have been neglected in our analysis.

It is clear from Figure 2b that systems exhibiting a large value of the ionic part of the dielectric constant, in general, have large dipole moments. However, the bond dipole moments alone are not sufficient to describe the calculated values of the ionic part of the dielectric constant and one has to also take into account information about the relative ease of reorientation of the structural units in a system. To, at least qualitatively, capture the ability of reorientation of the side chain dipoles around the backbone axis, we use tabulated energy barriers for rotation ($\xi_{XX'}$) about an X−X′ bond for homonuclear and heteronuclear homologues of ethane (i.e., XH_3−$X'H_3$; where X and X′ ∈ {C, Si, Ge, Sn}).[45,67] In Figure 2c, we plot $\mathcal{I}$, as defined below,

$$\mathcal{I} = \sum_i\left(\frac{2\mu_i}{\xi^i_{XX'} + \xi^i_{XX''}}\right) \tag{4}$$

against the ionic part of the dielectric constant, where the summation extends over all the backbone atoms and the X′ and X″ represent the two nearest backbone neighbors of atom X.

We note that among all the X−Y bonds, Sn−F has the largest dipole moment; at the same time, the Sn−Sn bond is the softest. Therefore, the large values of $\mathcal{I}$ in the Figure 2c are achieved for systems containing consecutive SnF_2 units, which is in agreement with the fact that the $-(CH_2)-(SnF_2)_3-$ motif in Figure 1d shows the highest value of the total dielectric constant, derived mostly due to a large lattice contribution. Considering that the distortion polarization and the dipole moments due to the backbone bonds are completely neglected, the correlation between the DFT calculations and the simple model based on just the atomic properties is rather respectable.

Thus, while the electronic part of the dielectric constant is mainly governed by the atomic polarizability and the vdW volume of the constituents and diminishes inversely with the bandgap, the large lattice contributions to the dielectric permittivity is contingent upon the availability of large and flexible dipole units in the structure. This elementary analysis provides us with intuitive "design pathways" for the creation of insulators with enhanced dielectric properties.

B. High Throughput Screening Strategy. Although the direct application of DFT methods provides a robust prescription for the computation of relevant dielectric properties, it is practically limited to polymer systems with a small periodic chain length. For longer chains (required to screen a larger part of the compositional and configurational space), the computational cost associated with DFT computations rises quite rapidly. Furthermore, as the system size increases, the number of candidates to be explored grows exponentially leading to a combinatorial explosion.

For instance, doubling the supercell size along the chain direction so as to include 8 distinct building units in a periodic repeating unit (while retaining every fourth unit to be CH_2 to be consistent with the 4-unit structures considered above) leads to a total of 29 365 different symmetry unique systems. Clearly, exploration of such a vast chemical space using the present first principles based approach may be impractical. Here, we investigate this large class of systems using an extension of the concept of additive group contributions,[43,68] involving parameters determined using the DFT results presented above.

According to the additive group contributions approach, a physical property of a polymer can be predicted by a sum of contributions made by the building units of the polymer. This assumption, however, is valid only when the influence of any one group in a structural unit of a polymer is mostly *local*. In other words, the group contribution approach is expected to work well only when contribution of a given group toward a certain property is not affected by the nature of the other groups present in the polymer. If there is mutual interaction between the units, a reliable prediction strategy requires one to go beyond the *on-site* group contributions and to include many body (i.e., two-body, three-body, etc.) interaction terms as well. This approach is what we refer to as the *modified additive group contributions* approach.

Within the modified additive group contributions approach (reminiscent of the cluster expansion scheme),[69−71] a certain property ζ of a given polymer chain can be written as a series of onsite and interaction contribution terms arising from interactions between various groups in the chain, as follows:

$$\zeta = \sum_i^N\{\sum_j n(i,j)\alpha_j^\zeta + \sum_{j,j'} n(i,j)n(i+1,j')\beta^\zeta_{jj'} + \sum_{j,j',j''} n(i,j)n(i+1,j')n(i+2,j'')\gamma^\zeta_{jj'j''}\} \tag{5}$$

where, the outer summation with index i is carried over all the different possible sites (N) in the backbone, while the index j in the inner summations runs over all the possible XY_2 unit types. Each of the site occupation numbers $n(i,j)$ is allowed to take a value of either one or zero, corresponding to whether the site i is occupied with the unit j or not. Furthermore, $\sum$ represents the summation over all the possible symmetry unique pairs or trios, within the applied periodic boundary conditions. The various onsite (α^ζ_j), two-body ($\beta^\zeta_{jj'}$), and three-body ($\gamma^\zeta_{jj'jj'}$) interaction contribution coefficients are then determined by fitting to the calculated DFT results. In principle, the above expression is a truncated version of an infinite series, which will include higher-order interactions terms. Retaining up to three-body interaction terms, the above expansion results in 175 different interaction contribution terms for each of the three properties (i.e., the bandgap, and electronic and total dielectric constants), which can be determined by fitting exactly to the results of the DFT calculations for the 175 systems. The 175 α^ζ_j, $\beta^\zeta_{jj'}$, and $\gamma^\zeta_{jj'jj'}$ interaction coefficients determined here are collected in Table 2 of the Supporting Information. A

dx.doi.org/10.1021/ci400033h | J. Chem. Inf. Model. 2013, 53, 879−886

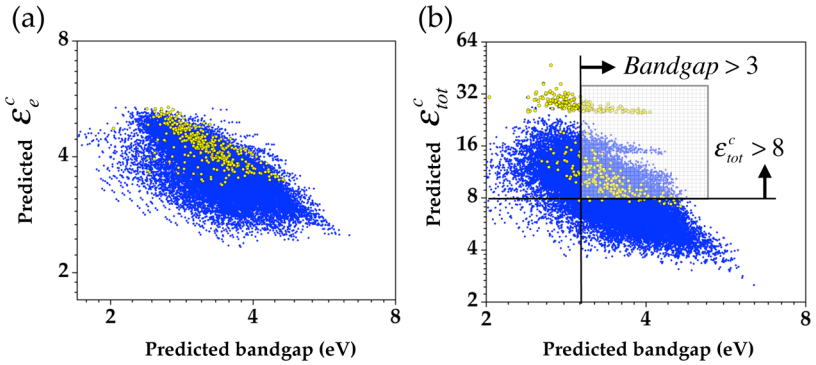

Figure 3. (a) ε^c_e and (b) ε^c_{tot} dielectric permittivities as a function of the bandgap predicted by the parametrization based on additive group contributions approach. In each of the two panels, systems containing three consecutive SnF_2 or GeF_2 units are highlighted. The region occupied by systems with simultaneously large bandgap (>3 eV) and ε^c_{tot} (>8) is partially shaded in panel b.

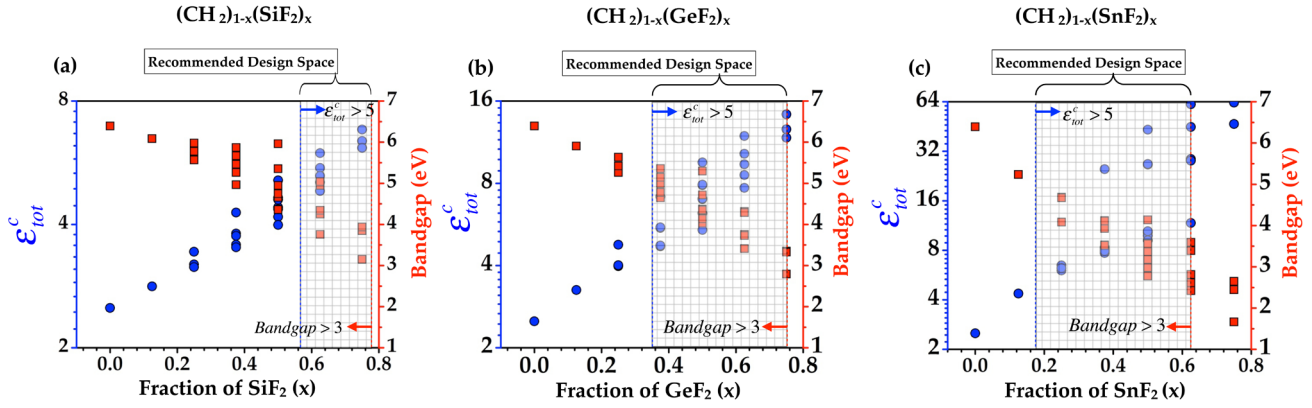

Figure 4. Variation between the ε^c_{tot} (with left axis and red color) and the bandgap (with right axis and blue color) as a function of composition x for (a) $(CH_2)_{1-x}-(SiF_2)_x$, (b) $(CH_2)_{1-x}-(GeF_2)_x$, and (c) $(CH_2)_{1-x}-(SnF_2)_x$ class of systems as predicted by the *property expansion* approach. A composition range corresponding to $\varepsilon^c_{tot} > 5$ and bandgap > 3 has been identified by hatching in each of the three panels.

comparison between the DFT-computed and the cluster expansion parametrization based predictions is provided in the Supporting Information and shows a satisfactory agreement between the two approaches.

We have employed the above parametrization strategy to compute the bandgaps, ε^c_e, and ε^c_{tot} for the aforementioned 29 365 eight-unit systems, which are plotted in Figure 3 (analogous to the plots shown in Figure 1). As encountered before, Figure 3a clearly shows that the Pareto optimal value of ε^c_e varies inversely with the bandgap. Therefore, the dielectric permittivity contributed due to electronic response alone is limited by the bandgap of the system. On the other hand, there appears no such limit on the lattice contribution of the dielectric constant.

In order to identify the "most promising" motifs that simultaneously exhibit large dielectric constant and bandgap values, we indicate in Figure 3b the region defined by the inequalities: bandgap > 3 eV and $\varepsilon^c_{tot} > 8$. Interestingly, this region is mostly constituted by systems containing fluorides in the backbone (i.e., SiF_2, GeF_2, and SnF_2). Furthermore, our analysis shows that the motifs with a large value of the ε^c_{tot} are composed of consecutive SnF_2 or GeF_2 units in the backbone. Systems containing three consecutive SnF_2 or GeF_2 units are highlighted in both Figures 3a and b. Furthermore, in addition to having a large ionic part of the dielectric constant, the identified systems also lie near the Pareto optimal front of the electronic part of the dielectric constant versus bandgap plot.

C. Guidelines for Synthesis. As the fluorides have been identified to be promising candidates thus far, we present a more focused analysis of the three subclasses of two-component systems of the type $(CH_2)_{1-x}-(XF_2)_x$, with X = Si, Ge, or Sn. The underlying motivation behind the specific choice of these systems also lies in their possible relative ease of synthesizability, as compared to the other complex multi-component systems considered in the above discussion. The predicted results of the bandgap and ε^c_{tot} on composition x for the three subclasses are captured in Figure 4a–c. In each of the three panels, a composition range (or the recommended design space) corresponding to $\varepsilon^c_{tot} > 5$ and bandgap > 3 eV has been highlighted to understand relative trends exhibited by the three subclasses of systems. In general, ε^c_{tot} (bandgap) increases (decreases) for a given composition as we go from the Si- to Ge- to Sn-based systems. Owing to this fact, the composition range highlighted in Figure 4 broadens and shifts toward the left as the dipole moments and relative ease of reorientation of the side chain atoms around the backbone increases. More importantly, Figure 4 provides further insights regarding the increasingly dominant role of the configuration in determining the bandgap and ε^c_{tot} as we move from Si- to Sn-based systems. For instance, for the 50% compositions, the largest value for ε^c_{tot} (and smallest value of bandgap) is achieved when like units are clustered, while an alternating arrangement of the CH_2 and XF_2 units leads to the lowest value of ε^c_{tot} (and largest value of bandgap) out of the several possible configurations. Furthermore, due to the increased tendency of σ-conjugation, the

dx.doi.org/10.1021/ci400033h | J. Chem. Inf. Model. 2013, 53, 879–886

difference between the smallest and the largest values of the ε^c_{tot} at $x = 0.5$ increases dramatically as we move from Si- to Ge- to Sn-based systems.

The findings presented above lead us to general recommendations concerning promising candidates that should exhibit large dielectric permittivity in combination with a large electronic bandgap. In general, while incorporation of SiF_2, GeF_2, and SnF_2 units in the polyethylene backbone is desirable to enhance the dielectric permittivity without sacrificing the excellent insulating properties, the chlorides of Si, Ge, and Sn lead to relatively lower bandgaps. The order of relative importance of fluorides in promoting the dielectric response is predicted to be $SiF_2 < GeF_2 < SnF_2$. Furthermore, owing to the increased tendency of σ-conjugation along the chains which in turn leads to an enhanced dielectric response, it is more desirable to have several concatenated, rather than well separated, SnF_2 or GeF_2 units (although below a critical number fraction to prevent drastic reduction of the bandgap) along a polymer chain in polyethylene. It is apparent from Figure 4 that to achieve a dielectric constant of 5 (i.e., more than double that of polyethylene) and a bandgap well above 3 eV, one will need to incorporate just about 17 mol % SnF_2 units in polyethylene (the corresponding values if GeF_2 or SiF_2 units are used turn out to be 35 or 55 mol %, respectively).

IV. CONCLUSIONS

In this first principles based computational study, the impact of incorporating various chemical motifs based on fluorides and chlorides of Si, Ge, and Sn on the dielectric permittivity of polyethylene has been investigated. The underlying trends in the dielectric constant and band gap computed using DFT for a manageable combination of polymer chains (totaling 175 cases) are explained by correlating the results with the tabulated data of various atomic properties. A much larger part of the of compositional and configurational space (composed of about 30 000 cases) was then investigated using the modified additive group contributions approach parametrized using the DFT data. Finally, based on the insights of the study, chemical motifs that may be incorporated in polyethylene to significantly enhance its dielectric constant without overly sacrificing its insulating properties (i.e., its bandgap) have been identified. The important findings of the present work could be summarized as follows:

- The electronic part of the dielectric constant is primarily determined by the sum of the atomic polarizability per unit van der Waals volume, while the lattice part of the dielectric constant is controlled by the value of the dipole moments that make up the system and the ease of their flexibility.
- Restrictions exist in the degree to which the electronic part of the dielectric constant can be enhanced. Owing to the apparent inverse relationship between the electronic part of the dielectric constant and the bandgap, improvement in the dielectric permittivity through a purely electronic response alone tends to degrade the insulating properties. Although the lattice part of the dielectric constant is also somewhat inversely correlated with the bandgap, it varies over a much larger range of values, and thereby provides more latitude.
- The motifs based on fluorides of Si, Ge, and Sn have been identified to be promising, in terms of enhancing the dielectric constant of polyethylene while still preserving a large enough bandgap. Origins of this improved dielectric response can be attributed to the relatively large polarizability per unit volume and availability of flexible dipole units of the fluoride units.
- Among the fluorides, motifs composed of consecutive SnF_2 units are predicted to be the most desirable. In addition to imparting extra flexibility to the polymer backbone, such motifs tend to locally enhance the σ-conjugation along the chains, which in turn leads to an increased dielectric response. However, there appears to be a minimum limit of about 17% for the mole fraction of SnF_2 that needs to be incorporated in polyethylene before any significant improvement on the dielectric permittivity is discernible.

Finally, we note that, while a fair amount of past synthesis work has been devoted to Si based polymers, experimental studies targeted toward organo-Ge and organo-Sn based polymers are very scarce in the literature to date. We hope that our systematic theoretical exploration would serve as a possible motivation for future experimental efforts along this direction.

■ ASSOCIATED CONTENT

Ⓢ Supporting Information

The optimized c lattice parameters, formation energies, bandgaps, the electronic part of the dielectric constant (ε^c_e), and the total dielectric constant (ε^c_{tot}) computed using DFT for the 175 systems comprising the 4-unit model are provided in Table 1. Table 2 contains the 175 interaction coefficients (α^ζ_j, $\beta^\zeta_{jj'}$, and $\gamma^\zeta_{jj'jj'}$) for each of the four properties. The validation parity plots, comparing DFT-computed and cluster expansion parametrized bandgaps as well as the electronic and ionic parts of dielectric permittivities for a limited set of eight-block systems are also provided. This material is available free of charge via the Internet at http://pubs.acs.org.

■ AUTHOR INFORMATION

Corresponding Author

*E-mail: rampi@ims.uconn.edu.

Notes

The authors declare no competing financial interest.

■ ACKNOWLEDGMENTS

This material is based upon work supported by a Multi-disciplinary University Research Initiative (MURI) grant from the Office of Naval Research. Computational support was provided through a National Science Foundation Teragrid Resource Allocation. Helpful discussions with Dr. Kenny Lipkowitz, Dr. Jeff Calame, and Dr. Vijay Kumar are also gratefully acknowledged.

■ REFERENCES

(1) Castelli, I. E.; Olsen, T.; Datta, S.; Landis, D. D.; Dahl, S.; Thygesen, K. S.; Jacobsen, K. W. Computational screening of perovskite metal oxides for optimal solar light capture. *Energy Environ. Sci.* **2012**, *5*, 5814−5819.

(2) Hautier, G.; Jain, A.; Ong, S. P. From the computer to the laboratory: materials discovery and design using first-principles calculations. *J. Mater. Sci.* **2012**, *47*, 7317−7340.

(3) Bennett, J. W. Discovery and Design of Functional Materials: Integration of Database Searching and First Principles Calculations. *Phys. Proc.* **2012**, *34*, 14−23.

(4) Yang, K.; Setyawan, W.; Wang, S.; Buongiorno Nardelli, M.; Curtarolo, S. A search model for topological insulators with high-throughput robustness descriptors. *Nat. Mater.* **2012**, *11*, 614−619.
(5) Curtarolo, S.; Setyawan, W.; Hart, G. L. W.; Jahnatek, M.; Chepulskii, R. V.; Taylor, R. H.; Wang, S.; Xue, J.; Yang, K.; Levy, O.; Mehl, M. J.; Stokes, H. T.; Demchenko, D. O.; Morgan, D. AFLOW: an automatic framework for high-throughput materials discovery. *Comput. Mater. Sci.* **2012**, *58*, 218−226.
(6) Curtarolo, S.; Setyawan, W.; Wang, S.; Xue, J.; Yang, K.; Taylor, R. H.; Nelson, L. J.; Hart, G. L. W.; Sanvito, S.; Buongiorno Nardelli, M.; Mingo, N.; Levy, O. AFLOWLIB.ORG: a distributed materials properties repository from high-throughput ab initio calculations. *Comput. Mater. Sci.* **2012**, *58*, 227−235.
(7) Wang, S.; Wang, Z.; Setyawan, W.; Mingo, N.; Curtarolo, S. Assessing the thermoelectric properties of sintered compounds with high-throughput ab-initio calculations. *Phys. Rev. X* **2011**, *1*, 021012.
(8) Hautier, G.; Jain, A.; Ong, S. P.; Kang, B.; Moore, C.; Doe, R.; Ceder, G. Phosphates as Lithium-Ion Battery Cathodes: An Evaluation Based on High-Throughput ab Initio Calculations. *Chem. Mater.* **2011**, *23*, 3495−3508.
(9) Mueller, T.; Hautier, G.; Jain, A.; Ceder, G. Evaluation of Tavorite-Structured Cathode Materials for Lithium-Ion Batteries Using High-Throughput Computing. *Chem. Mater.* **2011**, *23*, 3854−3862.
(10) Olivares-Amaya, R.; Amador-Bedolla, C.; Hachmann, J.; Atahan-Evrenk, S.; Sanchez-Carrera, R. S.; Vogt, L.; Aspuru-Guzik, A. Accelerated computational discovery of high-performance materials for organic photovoltaics by means of cheminformatics. *Energy Environ. Sci.* **2011**, *4*, 4849−4861.
(11) Setyawan, W.; Gaume, R. M.; Lam, S.; Feigelson, R. S.; Curtarolo, S. High-Throughput Combinatorial Database of Electronic Band Structures for Inorganic Scintillator Materials. *ACS Comb. Sci.* **2011**, *13*, 382−390.
(12) Hummelshøj, J. S.; Landis, D. D.; Voss, J.; Jiang, T.; Tekin, A.; Bork, N.; Dułak, M.; Mortensen, J. J.; Adamska, L.; Andersin, J.; Baran, J. D.; Barmparis, G. D.; Bell, F.; Bezanilla, A. L.; Bjork, J.; Björketun, M. E.; Bleken, F.; Buchter, F.; Bürkle, M.; Burton, P. D.; Buus, B. B.; Calborean, A.; Calle-Vallejo, F.; Casolo, S.; Chandler, B. D.; Chi, D. H.; Czekaj, I.; Datta, S.; Datye, A.; DeLaRiva, A.; Despoja, V.; Dobrin, S.; Engelund, M.; Ferrighi, L.; Frondelius, P.; Fu, Q.; Fuentes, A.; Frst, J.; Garcia-Fuent, A.; Gavnholt, J.; Goeke, R.; Gudmundsdottir, S.; Hammond, K. D.; Hansen, H. A.; Hibbitts, D.; Hobi, E.; Howalt, J. G.; Hruby, S. L.; Huth, A.; Isaeva, L.; Jelic, J.; Jensen, I. J. T.; Kacprzak, K. A.; Kelkkanen, A.; Kelsey, D.; Kesanakurthi, D. S.; Kleis, J.; Klpfel, P. J.; Konstantinov, I.; Korytar, R.; Koskinen, P.; Krishna, C.; Kunkes, E.; Larsen, A. H.; Lastra, J. M. G.; Lin, H.; Lopez-Acevedo, O.; Mantega, M.; Mart'ne, J. I.; Mesa, I. N.; Mowbray, D. J.; Mýrdal, J. S. G.; Natanzon, Y.; Nistor, A.; Olsen, T.; Park, H.; Pedroza, L. S.; Petzold, V.; Plaisance, C.; Rasmussen, J. A.; Ren, H.; Rizzi, M.; Ronco, A. S.; Rostgaard, C.; Saadi, S.; Salguero, L. A.; Santos, E. J. G.; Schoenhalz, A. L.; Shen, J.; Smedemand, M.; Stausholm-Møller, O. J.; Stibius, M.; Strange, M.; Su, H. B.; Temel, B.; Toftelund, A.; Tripkovic, V.; Vanin, M.; Viswanathan, V.; Vojvodic, A.; Wang, S.; Wellendorff, J.; Thygesen, K. S.; Rossmeisl, J.; Bligaard, T.; Jacobsen, K. W.; Nrskov, J. K.; Vegge, T. Density functional theory based screening of ternary alkali-transition metal borohydrides: A computational material design project. *J. Chem. Phys.* **2009**, *131*, 014101.
(13) Ortiz, C.; Eriksson, O.; Klintenberg, M. Data mining and accelerated electronic structure theory as a tool in the search for new functional materials. *Comput. Mater. Sci.* **2009**, *44* (4), 1042−1049.
(14) Greeley, J.; Nørskov, J. K. Combinatorial density functional theory-based screening of surface alloys for the oxygen reduction reaction. *J. Phys. Chem. C* **2009**, *113* (12), 4932−4939.
(15) Greeley, J.; Nørskov, J. K. Large-scale, density functional theory-based screening of alloys for hydrogen evolution. *Surf. Sci.* **2007**, *601*, 1590−1598.
(16) Madsen, G. K. H. Automated search for new thermoelectric materials: the case of LiZnSb. *J. Am. Chem. Soc.* **2006**, *128* (37), 12140−12146.
(17) Andersson, M. P.; Bligaard, T.; Kustov, A.; Larsen, K. E.; Greeley, J.; Johannessen, T.; Christensen, C. H.; Nørskov, J. K. Toward computational screening in heterogeneous catalysis: Pareto-optimal methanation catalysts. *J. Catal.* **2006**, *239*, 501−506.
(18) Greeley, J.; Jaramillo, T.; Bonde, J.; Chorkendorff, I.; Nørskov, J. K. Computational high-throughput screening of electrocatalytic materials for hydrogen evolution. *Nat. Mater.* **2006**, *5*, 909−913.
(19) Greeley, J.; Mavrikakis, M. Alloy catalysts designed from first-principles. *Nat. Mater.* **2004**, *3*, 810−815.
(20) Linic, S.; Jankowiak, J.; Barteau, M. A. Selectivity driven design of bimetallic ethylene epoxidation catalysts from first principles. *J. Catal.* **2004**, *224*, 489−493.
(21) Vitos, L.; Korzhavyi, P. A.; Johansson, B. Stainless steel optimization from quantum mechanical calculations. *Nat. Mater.* **2003**, *2*, 25−28.
(22) Muller, R. P.; Philipp, D. M.; Goddard, W. A. Quantum mechanical-rapid prototyping applied to methane activation. *Top. Catal.* **2003**, *23*, 81−98.
(23) Toulhoat, H.; Raybaud, P. Kinetic interpretation of catalytic activity patterns based on theoretical chemical descriptors. *J. Catal.* **2003**, *216*, 63−72.
(24) Greeley, J.; Nørskov, J. K.; Mavrikakis, M. Electronic structure and catalysis on metal surfaces. *Annu. Rev. Phys. Chem.* **2002**, *53*, 319−348.
(25) Franceschetti, A.; Zunger, A. The inverse band-structure problem of finding an atomic configuration with given electronic properties. *Nature* **1999**, *402*, 60−63.
(26) Ceder, G.; Chiang, Y.-M.; Sadoway, D. R.; Aydinol, M. K.; Jang, Y.-I.; Huang, B. Identification of cathode materials for lithium batteries guided by first-principles calculations. *Nature* **1998**, *392*, 694−696.
(27) Besenbacher, F.; Chorkendorff, I.; Clausen, B. S.; Hammer, B.; Molenbroek, A. M.; Nørskov, J. K.; Stensgaard, I. Design of a Surface Alloy Catalyst for Steam Reforming. *Science* **1998**, *279*, 1913−1915.
(28) Barshaw, E. J.; White, J.; Chait, M. J.; Cornette, J. B.; Bustamante, J.; Folli, F.; Biltchick, D.; Borelli, G.; Picci, G.; Rabuffi, M. High Energy Density (HED) Biaxially-Oriented Poly-Propylene (BOPP) Capacitors For Pulse Power Applications. *IEEE Trans. Magn.* **2007**, *43*, 223−225.
(29) *Handbook of Low and High Dielectric Constant Materials and Their Applications*; Nalwa, H. S., Ed.; Academic Press: San Diego, CA, 1999.
(30) Chu, B.; Zhou, X.; Ren, K.; Neese, B.; Lin, M.; Wang, Q.; Bauer, F.; Zhang, Q. M. Dielectric Polymer with High Electric Energy Density and Fast Discharge Speed. *Science* **2006**, *313*, 334−336.
(31) Tortai, J. H.; Bonifaci, N.; Denat, A.; Trassy, C. Diagnostic of the self-healing of metallized polypropylene film by modeling of the broadening emission lines of aluminum emitted by plasma discharge. *J. Appl. Phys.* **2005**, *97*, 053304(1)−053304(9).
(32) Yang, C.; Irwin, P. C.; Younsi, K. The future of nanodielectrics in the electrical power industry. *IEEE Trans. Dielect. Electr. Insul.* **2004**, *11*, 797−807.
(33) Sarjeant, W. J.; Zirnheld, J.; MacDougall, F. W. Capacitors. *IEEE Trans. Plasma Sci.* **1998**, *26*, 1368−1392.
(34) Rabuffi, M.; Picci, G. Status quo and future prospects for metallized polypropylene energy storage capacitors. *IEEE Trans. Plasma Sci.* **2002**, *30*, 1939−1942.
(35) Lovinger, A. J. Ferroelectric Polymers. *Science* **1983**, *220*, 1115−1121.
(36) *Organic Electronics: Materials, Processing, Devices and Applications*; So, F., Ed.; CRC Press: Boca Raton, FL, 2009.
(37) Ortiz, R. P.; Facchetti, A.; Marks, T. J. High-k organic, inorganic, and hybrid dielectrics for low-voltage organic field-effect transistors. *Chem. Rev.* **2010**, *110* (1), 205−239.
(38) Wang, C.; Dong, H.; Hu, W.; Liu, Y.; Zhu, D. Semiconducting π-Conjugated Systems in Field-Effect Transistors: A Material Odyssey of Organic Electronics. *Chem. Rev.* **2012**, *112*, 2208−2267.
(39) Wang, C. C.; Ramprasad, R. Dielectric properties of organosilicons from first principles. *J. Mater. Sci.* **2011**, *46*, 90−93.

(40) Wang, C. C.; Pilania, G.; Ramprasad, R. Dielectric properties of carbon-, silicon-, and germanium-based polymers: A first-principles study. *Phys. Rev. B* **2013**, *87*, 035103.
(41) Sun, Y.; Boggs, S. A.; Ramprasad, R. The intrinsic electrical breakdown strength of insulators from first principles. *Appl. Phys. Lett.* **2012**, *101*, 132906(1)−132906(5).
(42) Sun, Y.; Bealing, C.; Boggs, S. A.; Ramprasad, R. 50+ years of intrinsic breakdown. *IEEE Electr. Insul. M* **2013**, *29*, 8−15.
(43) Van Krevelen, D. W. *Properties of Polymers*; Elsevier: New York, 1990.
(44) *Silicon Polymers*; Muzafarov, A. M., Ed; Springer-Verlag: Berlin Heidelberg, Germany, 2011.
(45) *The Chemistry of Organic Germanium, Tin and Lead Compounds*; Patai, S., Ed.; John Wiley & Sons: New York, 1995; Vol. *1*.
(46) *The Chemistry of Organic Germanium, Tin and Lead Compounds*; Rappoport, Z., Ed.; John Wiley & Sons: New York, 2002; Vol. *2*.
(47) Tanke, R. S.; Kauzlarich, S. M.; Patten, T. E.; Pettigrew, K. A.; Murphy, D. L.; Thompson, M. E.; Lee, H. W. H. Synthesis of Germanium Nanoclusters with Irreversibly Attached Functional Groups: Acetals, Alcohols, Esters and Polymers. *Chem. Mater.* **2003**, *15*, 1682−1689.
(48) Hohenberg, P.; Kohn, W. Inhomogeneous Electron Gas. *Phys. Rev.* **1964**, *136*, B864−B871.
(49) Kohn, W.; Sham, L.; Self-Consistent, L. Equations Including Exchange and Correlation Effects. *Phys. Rev.* **1965**, *140*, A1133−A1138.
(50) Martin, R. *Electronic Structure: Basic Theory and Practical Methods*; Cambridge University Press: New York, 2004.
(51) Perdew, J.; Burke, K.; Ernzerhof, M. Generalized Gradient Approximation Made Simple. *Phys. Rev. Lett.* **1996**, *77*, 3865−3868.
(52) Kresse, G.; Furthmuller, J. Efficiency of ab-initio total energy calculations for metals and semiconductors using a plane-wave basis set. *Comput. Mater. Sci.* **1996**, *6*, 15−50.
(53) Blöchl, P. Projector augmented-wave method. *Phys. Rev. B* **1994**, *50*, 17953−17979.
(54) Baroni, S.; de Gironcoli, S.; Dal Corso, A. Phonons and related crystal properties from density-functional perturbation theory. *Rev. Mod. Phys.* **2001**, *73*, 515−562.
(55) Gonze, X.; Lee, C. Dynamical matrices, Born effective charges, dielectric permittivity tensors, and interatomic force constants from density-functional perturbation theory. *Phys. Rev. B* **1997**, *55*, 10355−10368.
(56) Pilania, G.; Ramprasad, R. Dielectric permittivity of ultrathin $PbTiO_3$ nanowires from first principles. *J. Mater. Sci.* **2012**, *47*, 7580−7586.
(57) Choy, T. C. *Effective medium theory: principles and applications*; Oxford University Press Inc.: Oxford, UK, 1999.
(58) Osborn, J. A. Demagnetizing Factors of the General Ellipsoid. *Phys. Rev.* **1945**, *67*, 351−357.
(59) Stoner, E. C. The demagnetizing factors for ellipsoids. *Phil. Mag.* **1945**, *36*, 803−821.
(60) Landau, L. D.; Lifshitz, E. M.; Pitaevskii, L. P. *Electrodynamics of Continuous Media*, second ed.; Course of Theoretical Physics; Pergamon Press: Oxford, 1984; Vol. *8*.
(61) Asaki, M. L. T.; Redondo, A.; Zawodzinski, T. A.; Taylor, A. J. Dielectric relaxation and underlying dynamics of acetonitrile and 1-ethyl-3-methylimidazolium triflate mixtures using THz transmission spectroscopy. *J. Chem. Phys.* **2002**, *116*, 10377−10385.
(62) Billmeyer, F. W. Lattice Energy of Crystalline Polyethylene. *J. Appl. Phys.* **1957**, *28*, 1114−1118.
(63) Pilania, G.; Zhu, H.; Ramprasad, R. Applications of Modern Density Functional Theory to Surfaces and Interfaces. In *A Matter of Density: Exploring the Electron Density Concept in the Chemical, Biological, and Materials Sciences*; Sukumar, N., Ed.; John Wiley & Sons, Inc.: New Jersey, 2012; pp 271−312.
(64) Zhu, H.; Tang, C.; Fonseca, L. R. C.; Ramprasad, R. Recent progress in ab initio simulations of hafnia-based gate stacks. *J. Mater. Sci.* **2012**, *47*, 7399−7416.
(65) Gajdoš, M.; Hummer, K.; Kresse, G.; Furthmüller, J.; Bechstedt, F. Linear optical properties in the projector-augmented wave methodology. *Phys. Rev. B* **2006**, *73*, 045112(1)−045112(9).
(66) Pauling, L. *General Chemistry*; Dover Publications Inc.: New York, 1988.
(67) Schleyer, P. V. R.; Kaupp, M.; Hampel, F.; Bremer, M.; Mislow, K. Relationships in the Rotational Barriers of All Group 14 Ethane Congeners H_3X-YH_3 (X,Y = C, Si. Ge, Sn, Pb). Comparisons of ab Initio Pseudopotential and All- Electron Results. *J. Am. Chem. Soc.* **1992**, *114*, 6791−6797.
(68) Yang, C.-J.; Jenekhe, S. A. Group Contribution to Molar Refraction and Refractive Index of Conjugated. Polymers. *Chem. Mater.* **1995**, *7*, 1276−1285.
(69) Sanchez, J. M. Cluster expansions and the configurational energy of alloys. *Phys. Rev. B* **1993**, *48*, 14013−14015.
(70) Sanchez, J. M. Cluster expansion and the configurational theory of alloys. *Phys. Rev. B* **2010**, *81*, 224202(1)−224202(13).
(71) Dalton, A. S.; Belak, A. A.; Van der Ven, A. Thermodynamics of Lithium in TiO_2(B) from First Principles. *Chem. Mater.* **2012**, *24*, 1568−1574.